Proposal to observe path superpositions in a double-slit setup

Q. Duprey
ENSEA, 6 Avenue du Ponceau, 95014 Cergy-Pontoise Cedex, France

A. Matzkin
Laboratoire de Physique Théorique et Modélisation, CNRS Unité 8089, CY Cergy Paris Université, 95302 Cergy-Pontoise Cedex, France

(Received 6 January 2022; revised 29 April 2022; accepted 9 May 2022; published 31 May 2022)

The interference pattern produced by a quantum particle in Young's double-slit setup is attributed to the particle's wave function having gone through both slits. In the path integral formulation, this interference involves a superposition of paths, going through either slit, linking the source to the detection point. We show how these paths superpositions can in principle be observed by implementing a series of minimally perturbing weak measurements between the slits and the detection plane. We further propose a simplified protocol in order to observe these "weak trajectories" with single photons.

DOI: 10.1103/PhysRevA.105.052231

I. INTRODUCTION

The weak measurement (WM) scheme [1] is a minimally disturbing process that enables one to gain information on the property of a quantum system at an intermediate time t as the system evolves from an initially prepared state $|\psi(t_i)\rangle$ to a state $|\chi(t_f)\rangle$ obtained as the result of a projective measurement at time t_f. More specifically, the WM of an observable $\hat{O}$ is achieved by introducing a weak coupling at an intermediate time of the evolution: a dynamical variable of the quantum pointer is weakly coupled at time t to the observable $\hat{O}$ of the system (a quantum particle) such that the probability of transition between the initial ("preselected") state $|\psi(t_i)\rangle$ and the detected ("postselected") state $|\chi(t_f)\rangle$ remains unchanged relative to the no-coupling case. When the final measurement at $t = t_f$ projects the system to state $|\chi(t_f)\rangle$, the weak value of $\hat{O}$ can be read by measuring the quantum pointer. The weak value O_w is a complex quantity given by

$$O^w(t) = \frac{\langle\chi(t_f)|\hat{U}(t_f,t)\hat{O}\hat{U}(t,t_i)|\psi(t_i)\rangle}{\langle\chi(t_f)|\hat{U}(t_f,t_i)|\psi(t_i)\rangle}, \tag{1}$$

where $\hat{U}(t',t)$ denotes the evolution operator of the system from t to t'. Typically, the momentum of the pointer is coupled to $\hat{O}$, in which case it can be shown [1,2] that the initial pointer state is shifted by a quantity proportional to Re O^w.

When $\hat{O}$ is given by the position operator $\hat{X}$, or by the projection to a particular spatial position $\Pi_x \equiv |x\rangle\langle x|$, the weak value captures information about the position of the system as it evolves between the pre- and postselected states. By inserting in different spatial regions a series of weakly coupled pointers that can be turned on and off at the desired time, it is possible to define "weak trajectories" [3]. Such trajectories are in principle observable signatures of the space-time evolution of the system. In simple cases, e.g., with narrow coherent states [3,4] or with pointlike pre- and postselected states [5] and free propagation, the system is seen to follow a classical trajectory, or a superposition of such trajectories.

This is reminiscent of Feynman's path integral approach [6], in which the evolution operator can be written (for free propagation, or when the potential is linear or quadratic in x) as a sum over classical paths [7]. In more complex situations [8–13], several Feynman paths compatible with pre- and postselection can interfere at the position of a weakly coupled probe, and may even result in a vanishing weak value (e.g., [14]). In a generic situation, Feynman paths interfere as the system evolves, so that reconstructing a weak trajectory from observed pointers is expected to be a difficult task.

The double-slit interferometer is arguably the simplest system displaying interference of Feynman paths: a point on the detection screen involves interferences between two paths, one coming from each slit. Aspects of weak trajectories in a double-slit setup were recently investigated [5,9,10] from an ideal point of view (pointlike pre- and postselected states, absence of weakly coupled pointers). In this work, we will propose a protocol to observe weak trajectories in view of a possible future experimental implementation with single photons. Indeed, the weak coupling of a quantum particle with an array of independent quantum pointers looks hardly feasible with current technologies. However, weak measurements have been successfully implemented on single photons by employing couplings with their polarization degree of freedom instead of genuine quantum pointers; this was done in particular in a double-slit setup that measured the velocity field of single photons [15], related to the weak value of the momentum.

Similarly, we will present here a protocol in order to detect with weak measurements the paths superposition contained in the Feynman propagator in a double-slit interferometer. We will first briefly review the free Feynman propagator and the associated paths for a double-slit setup (Sec. II). We will then introduce in Sec. III weak trajectories in an ideal scenario

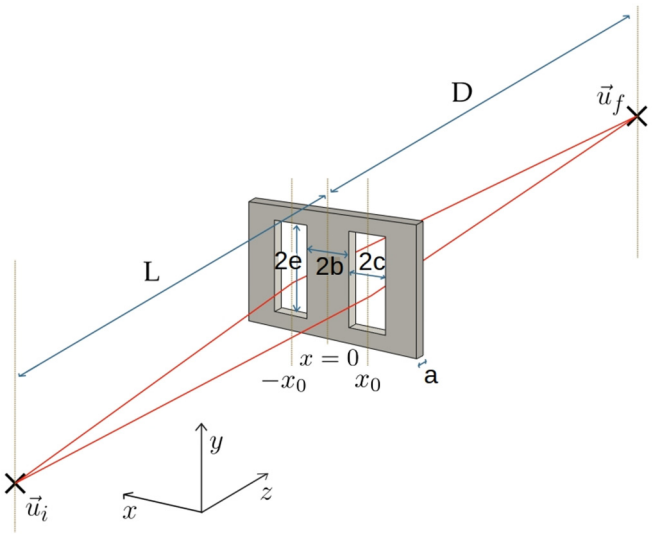

FIG. 1. Young's double-slit setup, introducing the notation employed in the text.

in which the wave function at each slit can be controlled, and then weakly interacts with a series of probes. This ideal scenario is useful in order to illustrate in a simple manner the superposition of weak trajectories. In a genuine double-slit setup, however, the wave front is carried by a sum over many interfering paths; how the corresponding weak trajectories could in principle be recovered by relying on weak measurements is studied in Sec. IV. Such a scheme is probably not realizable with current technologies. We therefore introduce (Sec. V) a protocol having in mind photonic experiments for which it should be possible to observe weak trajectories with currently available tools. This protocol is based on the interaction between a single photon and a minimal number of birefringent crystals placed between the slits and the detection screen. We discuss our results and conclude in Sec. VI.

II. FEYNMAN PATHS AND PROPAGATOR IN A DOUBLE-SLIT INTERFEROMETER

Let us consider Young's double-slit setup represented in Fig. 1. A particle is emitted at time t_i by a point source located at $\vec{u}_i$ and detected at time t_f at point $\vec{u}_f$ of a screen. The slits of width $2c$ and of thickness a are centered on $\pm x_0$, where $2x_0 = 2b + c$. We base our treatment on the approximations that are usually made [16–18] in this problem, namely,

(i) The slits are sufficiently long in the y direction so that diffraction effects along that direction can be neglected (hence only the propagator in the xz plane becomes relevant).

(ii) The xz propagation is factored into a plane-wave propagation along z and a propagator along x. This approximation, sometimes known as the truncation approximation [19], is justified in the Fraunhofer regime ($L \gg c$) and when the particle momentum is essentially along z ($|p_z| \gg |p_x|$).

(iii) The thickness a is deemed negligible, and the contribution of the loop trajectories [20,21] (going several times through the slits) are not taken into account.

Under these assumptions, the wave function of the problem is of the form $\Psi(x,z,t) = \psi(x,t)e^{ip_z z}e^{-i\frac{p_z^2}{2m}(t-t_i)/\hbar}$ and the relevant interference pattern is the one along the x direction. $\psi(x,t)$ is computed from the initial $\psi(x,t_i)$ through the propagator,

$$\psi(x',t') = \int_{-\infty}^{\infty} dx\, K(x',t'|x,t_i)\psi(x,t_i), \tag{2}$$

where

$$K(x',t'|x,t) \equiv \langle x'|e^{-i\frac{\hat{p}^2}{2m}(t'-t)}|x\rangle = \left(\frac{m}{2i\pi\hbar(t'-t)}\right)^{\frac{1}{2}} e^{\frac{im(x'-x)^2}{2\hbar(t'-t)}}, \tag{3}$$

is the propagator for the free Hamiltonian $\hat{H} = \hat{p_x}^2/2m$. Equation (3) is obtained from the path integral by "slicing" the evolution operator, and, as is well known [7], the result is that all the paths interfere destructively except the classical trajectory linking the point (x,t) to (x',t'). The phase in the exponent is the classical action $s(x',t')$ of that trajectory, while the amplitude of the propagator depends on the classical density $\partial^2 s/\partial x \partial x'$ of that trajectory.

We consider the slits as openings in a potential barrier. The functions $\varphi_1(x)$ and $\varphi_2(x)$ represent the shape of the slits 1 and 2 centered on x_0 and $-x_0$ respectively. Assuming a pointlike source, i.e., $\Psi(x_i,z_i,t_i) = \delta(x-x_i)\delta(z-z_i)$, the propagator from the source to a point (x_f,t_f) beyond the slits take the form

$$K(x_f,t_f|x_i,t_i) = \int_{-\infty}^{\infty} dx\, K(x_f,t_f|x,\tau)(\varphi_1(x) + \varphi_2(x))K(x,\tau|x_i,t_i) \tag{4}$$

$$= K_1(x_f,t_f|x_i,t_i) + K_2(x_f,t_f|x_i,t_i) \tag{5}$$

where we have defined $K_j(x_f,t_f|x_i,t_i) = \int_{-\infty}^{\infty} dx\, K(x_f,t_f|x,\tau)\varphi_j(x)K(x,t_f|x_i,t_i)$ to be the propagator associated with a passage through slit j at time τ.

For mathematical simplicity, we will take $\varphi_j(x)$ to be Gaussian functions $\varphi_1(x) = e^{-\frac{(x-x_0)^2}{2c^2}}$ and $\varphi_2(x) = e^{-\frac{(x+x_0)^2}{2c^2}}$ [16], rather than rectangular windows [17]. Taking $x_i = 0$ and $t_i = 0$, $K_j(x_f,t_f|x_i,t_i)$ becomes [16]

$$K_j(x_f,t_f|0,0) = \left\{\frac{m}{2i\pi\hbar[t_f + i\alpha\tau(t_f-\tau)]}\right\}^{\frac{1}{2}} \times \exp\left\{-\frac{1}{2(\Delta x)^2}(1-i\eta)\left(x_f - \delta_j x_0\frac{t_f}{\tau}\right)^2 + i\beta\frac{(x_f-\delta_j x_0)^2}{t_f-\tau} + i\beta\frac{x_0^2}{\tau}\right\}, \tag{6}$$

where

$$(\Delta x)^2 = \left(c\frac{t_f}{\tau}\right)^2 + \left(\frac{\hbar(t_f-\tau)}{mc}\right)^2, \quad \beta = \frac{m}{2\hbar}, \quad \alpha = \frac{\hbar}{mc^2}, \quad \eta = \frac{ct_f/\tau}{\hbar(t_f-\tau)/mc}, \quad \delta_{j=1} = +1, \quad \delta_{j=2} = -1. \tag{7}$$

The resulting probability at (x_f,t_f) is readily obtained from Eqs. (5) and (6). In the Fraunhofer approximation, Δx is greater than $\langle x_f\rangle$ and the probability at the screen $\mathcal{P}(x_f,t_f)$

can be approximated in the compact form [16]

$$\mathcal{P}(x_f, t_f) = \cos^2\left(\frac{2p_z x_0 x_f}{\hbar D}\right) e^{-\frac{x_f^2}{(\Delta x)^2}}, \tag{8}$$

where $p_z = mv_z = mD/(t_f - \tau)$.

This interference is due to the superposition of the two type of trajectories associated with Eq. (5): those that go from x_i to x_f through slit 1, and those that go through slit 2. In principle, there are an infinite number of classical trajectories associated with each propagator $K_j(x_f, t_f|x_i, t_i)$, each distinguished by a different intermediate point on the slit plane. Note, however, that Eq. (6) indicates that each K_j is essentially a Gaussian wave function that can be characterized by the classical trajectory followed by the maximum of the Gaussian, $x_j(t) = \delta_j x_0 + \frac{p_x^j}{m}(t - \tau)$.

III. AN IDEAL CASE: CONTROLLING PREELECTION AT THE SLITS

A. An array of weakly coupled pointers

We will see here how the superposition of paths going through each slit can be obtained in an ideal double-slit experiment in which a set of quantum pointers, disposed on a grid, may interact—weakly and unitarily—with the system (say a single electron) originating from the source, and detected on the screen. We will assume each probe is coupled to the spatial projection operator $\hat{\Pi}_a \equiv |\mathbf{r}_a\rangle\langle\mathbf{r}_a|$ of the system, where $\mathbf{r}_a = (x_a, z_a)$. The pre- and postselected states, to be specified later, will be denoted by $|\psi(t_i)\rangle$ and $|\chi(t_f)\rangle$ respectively. Applying the weak value definition (1) to $\hat{\Pi}_a$ for an interaction at time t gives

$$(\Pi_a)^w(t) = \frac{\langle\chi(t_f)|\hat{U}(t_f, t)\hat{\Pi}_a\hat{U}(t, t_i)|\psi(t_i)\rangle}{\langle\chi_f(t_f)|\hat{U}(t_f, t_i)|\psi(t_i)\rangle} \tag{9}$$

$$= \frac{\chi^*(x_a, t)\psi(x_a, t)}{\int dx \chi^*(x, t)\psi(x, t)} = (\Pi_{x_a})^w(t), \tag{10}$$

where $\hat{U}(t, t_i)$ is the free evolution operator. Note that, given the assumptions introduced in Sec. II, the evolution along the z axis is trivial, yielding phase factors that cancel out, so that only the weak value $(\Pi_{x_a})^w$ along x is relevant. We will not review here the properties of weak values (see, e.g., [22] for a recent review), though it should be recalled that $(\Pi_a)^w$ is complex valued and only the real part (inducing a shift on a pointer) is related to the property of the system observable $\hat{\Pi}_a$ coupled to the pointer.

The probes are organized on a grid as schematically shown in Fig. 2. Let us label each probe by $\mathcal{M}_{ab}$, where a stands for the position (x_a, z_a) and b for the time of interaction t_b. Let $|\xi_{a,b}\rangle$ denote the quantum state of the probe $\mathcal{M}_{ab}$. We will assume the interaction Hamiltonian between the system and each probe to be of the form

$$\hat{H}_{\text{int}}^{a,b} = g(t_b)\hat{\Pi}_a\hat{P}_a, \tag{11}$$

where $g(t_b)$ is the coupling strength (a smooth function peaked at t_b), and where $\hat{P}_a$ is a dynamical variable of probe $\mathcal{M}_{ab}$ (typically the momentum, but see below in Sec. V for a different choice). Setting $\int_{t_b-T/2}^{t_b+T/2} g(t')dt'/\hbar \equiv \gamma_b$ where T is the duration of the weak coupling, the evolution operator due to the weak coupling between the system and a probe becomes

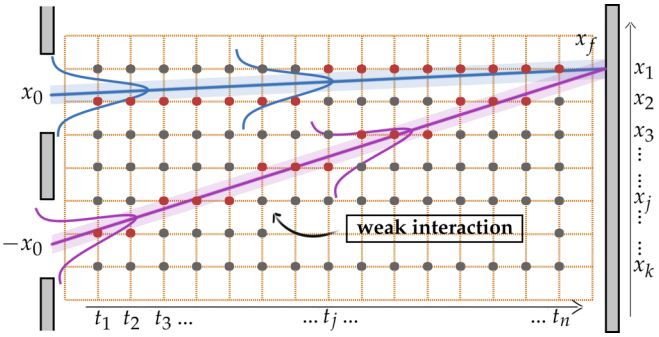

FIG. 2. Ideal two-slits setup with a grid of weakly coupled probes. A particle is initially in a superposition of coherent states at the slits. The coherent states are directed toward a point x_f on the screen. Each dot represents a probe that couples to the particle through a weak unitary interaction. Upon postselection, some probes see their quantum state shifted as a result of the weak interaction. Each set $\{t_k, \mathbf{r}_k\}$ of these shifted probes defines a "weak trajectory." With an appropriate choice of postselection, the weak trajectories shown here joining slit 1 to x_f and slit 2 to x_f can be detected jointly (see text for details)

$$\exp(-i\gamma_b\hat{\Pi}_a\hat{P}_a) \simeq 1 - i\gamma_b\hat{\Pi}_a\hat{P}_a. \tag{12}$$

The b subscript in γ_b is a label added in order to distinguish the interaction times wherever necessary (this has no bearing on the numerical values of all the γ_b's that will taken to be the same assuming identical probes). With this notation, taking for convenience $t = 0$ when the system wave function is at the slits, the overall quantum state, given initially by $|\Psi(t = 0)\rangle = |\psi(t = 0)\rangle \bigotimes_a |\xi_{a,b}(t = 0)\rangle$, becomes

$$|\Psi(t_f\rangle = \prod_{b=1}^{n}\left[\hat{U}(t_b, t_{b-1})\prod_{a=1}^{k} e^{-i\gamma_b\hat{\Pi}_a\hat{P}_a}\right]|\Psi(t = 0)\rangle, \tag{13}$$

with $t_0 = 0$ and $t_n = t_f$. Applying Eq. (12) and keeping only terms to first order in the couplings γ_b, and finally postselecting to the state $|\chi_f\rangle$ leaves the quantum state of each probe $\mathcal{M}_{ab}$ shifted in proportion to the corresponding weak value,

$$|\xi_{a,b}(t_f)\rangle = \exp(-i\gamma_b(\Pi_a)^w\hat{P}_a)|\xi_{a,b}(t = 0)\rangle. \tag{14}$$

In principle, the quantum state of each probe can be read out after postselection. From the knowledge of the position $\mathbf{r}_a$ of each probe and the control of the interaction time t_b, one can define "weak trajectories" by linking the probes for which $\text{Re}(\Pi_a)^w \neq 0$.

B. Controlling preselection at the slits

We have seen in Sec. II that a point source located behind Gaussian slits results in a Gaussian propagating from each slit. In this section we will introduce weak trajectories for slits in a slightly more general situation in which we assume the Gaussian wave functions emanating from the slits can be controlled.

To this end, consider the preselected state to be given by

$$\psi(x,t) = \frac{1}{\sqrt{2}}\left(\psi^1_{p_i^1}(x,t) + \psi^2_{p_i^2}(x,t)\right), \tag{15}$$

where the Gaussian

$$\psi^j(x,0) = \frac{1}{(2\pi d^2)^{\frac{1}{4}}} e^{-i\frac{(x-\delta_j x_0)^2}{4d^2} + i\frac{p_i^j(x-\delta_j x_0)}{\hbar}} \tag{16}$$

is the wave function for slit j (as above $\delta_j = +1$ for $j = 1$ and $\delta_j = -1$ for $j = 2$). p_i^j denotes the initial ($t = 0$) mean momentum along x of the slit j wave function, and as usual x_0 and d are the mean position and width of the Gaussian respectively. The free evolution of the Gaussian (16) is well known to be given [e.g., by applying the free propagator (3) to Eq. (16)] by

$$\psi^j(x,t) = \left(\frac{2}{\pi}\right)^{\frac{1}{4}} \frac{e^{-i\pi/4}}{\sqrt{\frac{\hbar t}{md} - 2id}} \times \exp\left\{-\frac{md^2\left((\delta_j x_0 - x) + p_i^j t/m\right)^2}{4d^4m^2 + \hbar^2 t^2} + i\frac{4d^4 m p_i^j\left(2mx - p_i^j t\right) + \hbar^2 t\left(m(x-x_0)^2 + 2p_i^j x_0 t\right)}{8d^4 hm^2 + 2\hbar^3 t^2}\right\}. \tag{17}$$

The maximum of $|\psi^j(x,t)|^2$ thus moves along the classical trajectory

$$x_i^j(t) = \delta_j x_0 + \frac{p_i^j}{m} t. \tag{18}$$

Note that if the Gaussian remains sufficiently narrow between the slits and the screen (that is narrower than the spatial resolution of the probes or screen detector), $\psi^j(x,t)$ can be said to be carried effectively by the single classical trajectory defined by Eq. (18). In this case the preselected state (15) involves two trajectories, with p_i^1 and p_i^2 chosen so that these two trajectories meet at some point, say x_1 on the detection screen (see Fig. 2).

C. Postselection

For the postselected wave function, the natural choice would be to select a position $|x_f\rangle$ on the detection screen, or more realistically a window function of the size of the spatial resolution. Rather than dealing with unit-step functions, we will work for simplicity with a Gaussian centered on x_f and further assume we can control by collimation the incoming mean momentum p'_k at the screen,

$$\Xi_{x_f,p'_k}(x,t_f) = \frac{1}{(2\pi\Delta^2)^{\frac{1}{4}}} e^{i\frac{(x-x_f)^2}{4\Delta^2} - i\frac{p'_k(x-x_f)}{\hbar}}. \tag{19}$$

where the width Δ is of the order of the spatial resolution of the detector. We will actually define for the controlled case studied here the postselected wave function to be given by a sum over such Gaussians all centered on x_f,

$$\chi_{x_f}(x,t_f) = \sum_k c_k\, \Xi_{x_f,p'_k}(x,t_f), \tag{20}$$

with weights c_k. The advantage of this choice is that the maximum of each $\Xi_{x_f,p'_k}(x,t)$ at a backward evolved time t can be seen to move, similarly to Eq. (17), along the classical trajectory

$$x'_k(t) = x_f + \frac{p'_j}{m}(t_f - t). \tag{21}$$

D. Weak trajectories

Assume a probe placed at $\mathbf{r}_a = (x_a, z_a)$ is weakly coupled to the system with the interaction Hamiltonian given by Eq. (11). The preselected state is given by Eq. (15), and let us take the postselected state to be given by Eq. (20) with a single term ($c_1 = 1$, $c_{k\neq 1} = 0$). If the evolving preselected state remains narrow, postselection can only be successful if the postselection position and momentum collimation are set to

$$x_f = \begin{cases} x_0 + p_i^1 t_f/m, \\ -x_0 + p_i^2 t_f/m, \end{cases} \qquad p'_k = \begin{cases} p_i^1, \\ p_i^2. \end{cases} \tag{22}$$

From Eqs. (9) and (10), we see that the weak value will be nonzero only if the probe is positioned on the classical trajectory between the slit and the postselection point, since otherwise $\chi^*(x_a)\psi(x_a) \approx 0$. If we assume an array of probes arranged as in Fig. 2, the same reasoning applies, now based on Eq. (14): given a final point, say the point $x_f = x_1$ shown in Fig. 2, each probe along the trajectory coming from slit 1 (blue colored on Fig. 2) will be shifted if postselection is chosen with $p'_k = p_i^1$. This set of shifted probes $\mathcal{M}_{ab}$ defines the weak trajectory given the pre- and postselected states. Similarly, if the postselected state is chosen so that $p'_k = p_i^2$, then only the probes along the red trajectory coming from slit 2 will be found to have shifted, defining the weak trajectory obtained with this different postselected state.

Finally, let us choose the postselected state to be given by Eq. (20) but now with $c_1 = c_2 = 1/\sqrt{2}$, $c_{k\neq 1,2} = 0$ and set $p'_1 = p_i^1$, $p'_2 = p_i^2$. Now the set of probes $\mathcal{M}_{ab}$ along the trajectories coming from both slits (the blue and the red trajectories of Fig. 2) will be detected to have shifted. With this choice of postselection we have obtained a superposition of weak trajectories, that could in principle be observed by monitoring the probes $\mathcal{M}_{ab}$. This superposition of weak trajectories can be understood as a sum over two effective Feynman paths.

IV. WEAK TRAJECTORIES IN A DOUBLE-SLIT SETUP

A. Overlapping wave fronts

A double-slit setup typically displays wide interfering wave fronts expanding from the slits to the screen instead of narrow wave packets propagating along one effective coarse-grained trajectory. Each wave front is carried by several paths

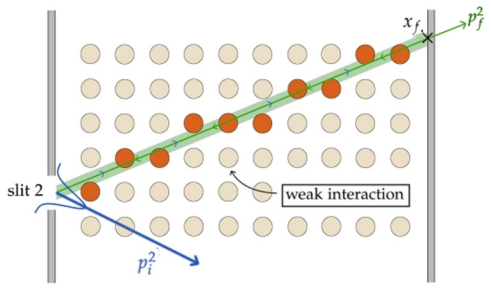

FIG. 3. Schematic representation (not to scale) of a grid of weakly coupled probes interacting with the particle sent from a source (placed at $x = 0$ as shown in Fig. 1), hence without control of the transverse momentum. Here only slit 2 is open and the postselected state is collimated to filter along the direction of the momentum p_2^f indicated by the arrow. The probes that have shifted after postselection are shown in darker tones.

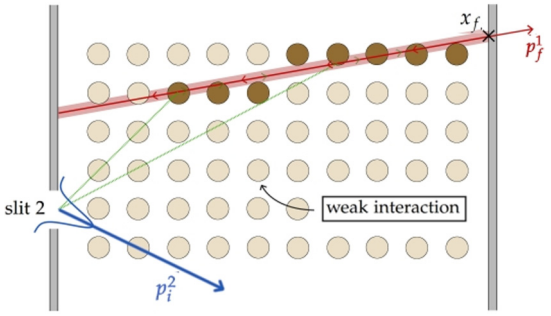

FIG. 4. Same as Fig. 3 but with a different collimation direction. The resulting weak trajectory only appears in the Fraunhofer region (see text for details).

emanating from the slits (recall here that, due to the factorization assumption of Sec. II, the wave front in the far field moves at constant speed p_z/m). Moreover several paths interfere at the location of a probe. Identifying weak trajectories in this context from a grid of weakly coupled probes is more involved than in the controlled case with narrow wave packets.

In this situation the wave function in the Fraunhofer region or at the detection screen is given by Eq. (6), that can be shown to be proportional to Eq. (17) with the replacements $t \to t - \tau$, $(\Delta x)^2 \to 2d^2 + \hbar^2 t^2/(2m^2 d^2)$ and $\tau \to m\delta_j x_0/p_i^j$. Hence we will set the preselected wave function to be again given by Eq. (15) except that now neither the width nor the initial momentum are controlled, but depend on the slit geometry and on the position of the source. We will still assume however that we can control the postselected state, by collimating the mean momentum of the particle incoming on the screen at x_f, and by choosing narrow window of detection [the parameter Δ in Eq. (19)]. Hence the postselected wave function is identical to Eq. (20).

B. Weak measurement of a single classical trajectory

Assume only one slit is open, say slit 2. In this case, the preselected wave function is given by

$$\psi_{p_i}^2(x,t) = \frac{1}{(2\pi d^2)^{\frac{1}{4}}} e^{-i\frac{(x+x_0)^2}{4d^2} + ip_i(x+x_0)/\hbar}, \tag{23}$$

[cf. Eq. (16)]. Let us set the postselected wave function $\chi_{x_f}(x,t) = \Xi_{x_f,p_f^2}(x,t)$ [cf. Eq. (20)] to be collimated along a single momentum p_f^2 chosen such that the classical trajectory emerging from the center of slit 2 reaches x_f at time t_f, as shown on Fig. 3. Hence

$$x_f^1(t_f) = x_0 + \frac{p_f^1}{m} t_f. \tag{24}$$

Let us place an array of probes $\mathcal{M}_{ab}$ as shown in Fig. 3. The probes weakly measure the projectors $\hat{\Pi}_a$ at times t_b. The weak values displayed by the weak detectors are given by

$$(\Pi_a)_w(t_b) = \frac{\chi_{x_f}^*(x_a,t_b)\psi_{p_i}^2(x_a,t_b)}{\int dx \chi_{x_f}^*(x,t_b)\psi_{p_i}^2(x,t_b)}, \tag{25}$$

where $\chi_{x_f}^*(x,t) = \Xi_{x_f,p_f^2}^*(x,t)$ is given by Eq. (19).

Sufficiently far from the slits (where the Fraunhofer approximation holds), $\psi_{p_i}^2(x_a,t_b)$ will be nonzero, except accidentally if x_a happens to lie on a node of the wave function; we discard this possibility since in practice the interaction does not take place at a single point but over a region centered on $\mathbf{r}_a$ [23]. Therefore $(\Pi_a)_w(t_b)$ will be nonzero only if $\mathbf{r}_a$ lies near the trajectory defined by the postselected momentum. If p_f^2 is chosen to be along the classical trajectory going from $-x_0$ (the center of slit 2) to x_f, then $(\Pi_a)_w \neq 0$ for all the probes $\mathcal{M}_{ab}$ in the neighborhood of that trajectory. This case, pictured in Fig. 3 is similar to the cases discussed in Sec. III, in which the weak trajectory links the slit to the postselection point.

However, we may pick p_f^2 along a different direction, as portrayed in Fig. 4. In this case, we know from the propagator [Eq. (3)] that $\chi_{x_f}^*(x_a,t_b)$ will be nonzero essentially along the backward evolved trajectory given by Eq. (21). The probes $\mathcal{M}_{ab}$ for values of t_b sufficiently large (that is far from the slits, where the wave front is approximately uniform along z) will therefore shift, but not those closer to the slits since for small values of t_b we have $\psi_{p_i}^2(x_a,t_b) \approx 0$ if x_a is appreciably different from $-x_0$. Such a situation gives rise to the "incomplete" weak trajectory shown in Fig. 4.

Finally, let us consider the two-slit situation with the same postselected state. Recalling that the initial wave function is given by Eq. (15), the weak value (25) resulting from the coupling of probe $\mathcal{M}_{a,b}$ now becomes

$$(\Pi_a)^w(t_b) = \frac{\chi_{x_f}^*(x_a,t_b)\left(\psi_{p_i^1}^1(x_a,t_b) + \psi_{p_i^2}^2(x_a,t_b)\right)}{\int dx \chi_{x_f}^*(x,t_b)\left(\psi_{p_i^1}^1(x,t_b) + \psi_{p_i^2}^2(x,t_b)\right)}. \tag{26}$$

Hence opening the second slit does not affect dramatically the weak trajectories; for instance for the choice of p_f^2 corresponding to Fig. 3, the weak trajectory does not change at all. However, the weak values do change, due to the contribution of the Feynman paths coming from the other slit (see Fig. 5). The difference between the weak values (25) and (26) can be understood as a signature of the interference (carried by additional paths) between the waves coming from each slit.

C. Weak measurement of several classical trajectories

One can measure several weak trajectories with a single open slit by employing a postselected state of the form (20), similarly to the case treated in Sec. III. The difference here is

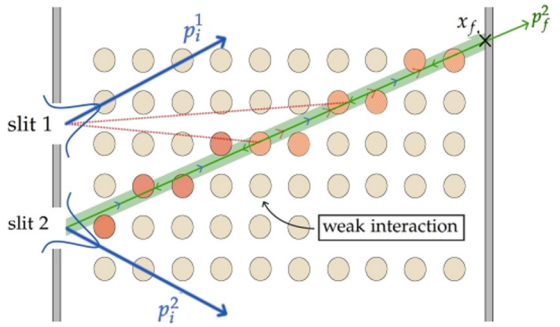

FIG. 5. Same as Fig. 3 but with both slits open. The shifts of some probes in the Fraunhofer region change due to the paths coming from slit 1 (they are pictured with a lighter tone), though the weak trajectory is the same as in Fig. 3.

that most weak probes will receive contributions from paths coming from each slit, as in the case described by Eq. (26). Let us take again the postselected state to be of the form given by Eq. (20),

$$\chi_{x_f}(x,t) = \frac{1}{\sqrt{2}}\left(\Xi_{x_f,p_f^1}(x,t) + \Xi_{x_f,p_f^2}(x,t)\right), \qquad (27)$$

where Ξ_{x_f,p_f^1} is defined by Eq. (19). The resulting weak values are given by replacing $\chi_{x_f}(x_a,t_b)$ with Eq. (27) in Eq. (26). This situation is portrayed in Fig. 6, in which p_f^1 and p_f^2 are chosen along the trajectories linking the slits 1 and 2 to x_f. The weak probes that will shift, defining the weak trajectories, are those between the slits and the detector at $\mathbf{r}_f$.

The difference with the ideal case discussed in Sec. III is that now trajectories from both slits reach each probe. This gives yet another signature, in terms of the weak values of the interference between the waves coming from each slit. These waves are carried by Feynman paths propagating along classical trajectories. For each weakly coupled probe, the weak value depends on three trajectories (or three families of trajectories if one takes into account the finite width of the weak probes and the screen detector): the trajectories from each slit to the probe and the trajectory from the probe to the postselected detector on the screen. If one slit is closed, ψ^1 or ψ^2 in Eq. (26) vanishes. This changes the weak values of the weak probes in the Fraunhofer region. Note that the weak

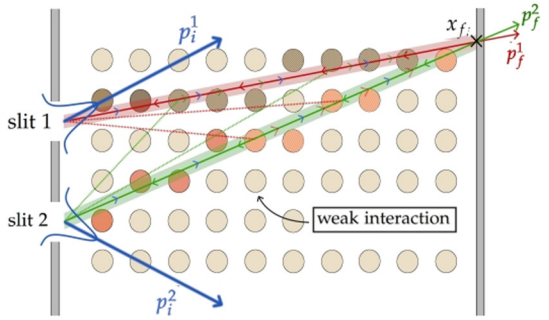

FIG. 6. Same as Fig. 5 but now the postselection filters along the directions p_f^1 and p_f^2 as indicated by the arrows pictured at x_f. The paths superposition is identical to the ideal case shown in Fig. 2 but here paths from both slits contribute to the weak value of most probes.

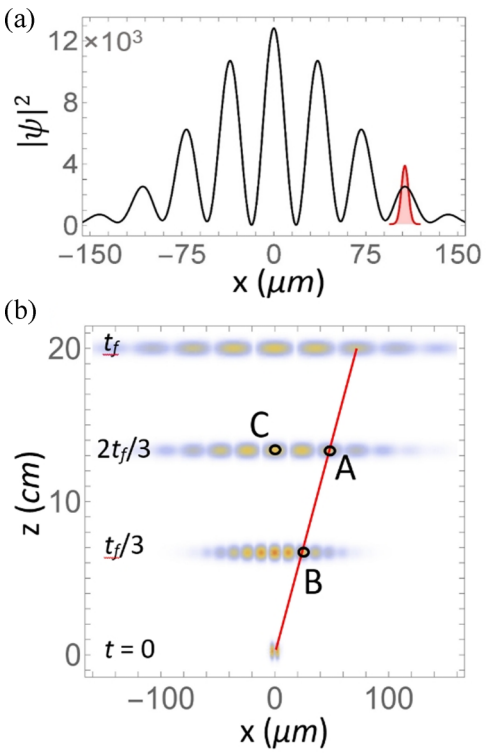

FIG. 7. (a) Interference pattern due to electron diffraction on a detection plane placed 20 cm from the slits (see text for the parameter values). The postselected state is represented as a filled peak (in red). (b) Snapshots of the electron density as the electron evolves from the slits (at $t = 0$) to the detector (at $t = t_f$). The chosen postselected state filters the wave function traveling along the red trajectory going through the points A and B. The weak values at the positions A, B, and C are given in Table I.

probes closer to the shut slit will have null weak values, since both ψ^1 and ψ^2 will vanish at the location of the weak probes.

D. Numerical illustration

We present here an illustration with numbers corresponding to current typical single electron diffraction experiments,; see, e.g., Ref. [24]. In such experiments the slit plane dimensions is in the mesoscopic range, while the interference figure is of macroscopic size. This leaves ample room to insert pointers between the plane and detector planes, though discriminating the postselection between p_f^1 and p_f^2 as in Eq. (27) becomes unpractical, since $p_f^1 \approx p_f^2$.

Figure 7(a) shows the interference pattern on a detection screen placed 20 cm from the slit plane (we thus have [refer to Fig. 1 and Eqs. (16)–(18)] $m = m_e \approx 9.1 \times 10^{-31}$ kg, $D = 0.2$ m, and the other parameter values are $x_0 = 2$ μm, $d = 0.2\mu$m, $p_i^1/m = -p_i^2/m = 100$ m/s, $p_z/m = 10^6$ m/s), obtained by evolving Eq. (15) up to $t_f = mD/p_z = 0.2$ μs. We also show in Fig. 7(a) the postselected state (19) at $t = t_f$, choosing $x_f = 109.9$ μm at the maximum of the third peak to the right of the central peak of the diffraction figure. The postselected momentum is chosen along the direction of slit 1, $p_f^1 = m(x_f - x_0)/t_f$. We set $\Delta = 2$ μm.

Figure 7(b) shows a density plot of the electron wave function as the electron evolves from the slits to the detection

TABLE I. Real part of the spatial projector weak value at points A, B, and C shown in Fig. 7(b). Different cases with slits open or closed are considered, giving rise to different weak values.

	A ($t = 2t_f/3$)	B ($t = t_f/3$)	C (any t)
Both slits open	0.38	4.26	0
Slit 1 (x_0) open only	−1.79	8.18	0
Slit 2 ($-x_0$) open only	0.75	1.51	0

screen. We also indicate three positions A, B, and C for which we compute weak values given in Table I. The weak values are computed using an expression of the type given by Eq. (25) when only one slit is open, or Eq. (26) when both slits are open. We integrate the numerator in Eqs. (25) and (26) with the same smooth Gaussian [23] to take into account the finite width of the coupling. The results for the real part of the weak values are shown in Table I. It can be seen that the weak values are markedly different depending on which slit is open. The last column (for a weak pointer C) is meant to illustrate that any weak value will vanish if it does not lie along the trajectory defined by the postselected state [the red line in Fig. 7(b)].

V. SIMPLIFIED PROTOCOL FOR A PHOTONIC IMPLEMENTATION

A. Overview

In this section, we detail a concrete protocol to measure weak trajectories, having in mind a photonic setup, in the line of recent experiments dealing with single photons going through slits [15,25]. The protocol is a simplified version of the double-slit setup case seen in the previous section (Sec. IV).

The main difference with the previous setups is that the weak probes are not independent systems that couple to the photon, but optical elements that create a coupling between the spatial degree of freedom of the photon and its polarization. The result of the coupling is encoded in the photon itself. Hence it is not possible to imagine a dense array of probes whose state would be read out after postselection. Here, in order to extract the rotations due to the weak coupling with the optical elements, we need to implement a protocol with a small number of glass plates or birefringent crystals placed between the slits and the detector screen. In the present protocol, we will work with birefringent crystals coupling at a given position the transverse momentum along x, $\hat{k}$ to the photon polarization. We will therefore deal with the corresponding weak values $(k)^w$ of the transverse momentum, instead of the weak values of the position $\hat{\Pi}_a$.

Nevertheless, we will see that the weak measurement of $\hat{k}$ allows us to observe the superposition of trajectories. The rationale is that a non-null weak value implies that the photonic wave has interacted with the birefringent crystal. The weak probe is now the photon polarization, which is rotated (rather than shifted) by a quantity proportional to $(k)^w$. Reading out the polarization at postselection allows us to infer the past interactions of the photon with the birefringent crystals, and from there to reconstruct the weak trajectories.

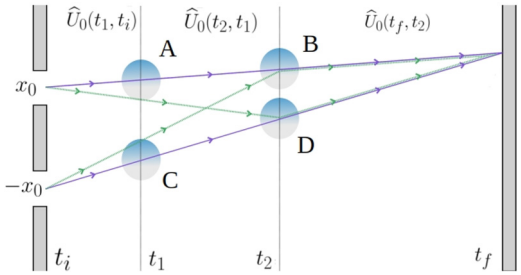

FIG. 8. Schematic diagram (not to scale) showing four birefringent crystals creating a weak coupling in order to measure the paths superposition in a photonic setup. A and B are disposed near the slits while B and D are located in the Fraunhofer region. The paths joining the slits to the crystals and to x_f (the postselected position on the detection screen) are the weak trajectories inferred from the measurement of the polarization intensities.

B. Interactions and weak values

Consider the setup represented in Fig. 8. Two of the birefringent crystals (A and C) are near the slits (in the region with spherical wave fronts) while B and D are in the Fraunhofer region. The preselected state is again of the form given by Eqs. (15)–(16), where the mean momentum of each Gaussian is not controlled but depends on the relative positions of the source and the slits plane, as in Sec. IV. The initial polarization is chosen to be diagonal, $|\nearrow\rangle = (|H\rangle + |V\rangle)/\sqrt{2}$, so the photon state at the slits is (setting $t = 0$ when the photon wave function crosses the slits)

$$\frac{1}{\sqrt{2}}\left(\psi^1_{p_i^1}(x,0) + \psi^2_{p_i^2}(x,0)\right)|\nearrow\rangle. \tag{28}$$

The interaction Hamiltonian between the photon wave function and a birefringent crystal is given by

$$\hat{H}_a = g_a \hat{k}\hat{\sigma}_\alpha, \tag{29}$$

where g_a is the coupling constant and $\hat{\sigma}_\alpha = \frac{\hbar}{2}\hat{\Pi}_a\sigma_3$ is the linear polarization observable at the position (x_a, z_a) of the crystal ($\sigma_3 = |H\rangle\langle H| - |V\rangle\langle V|$ is the third Pauli matrix). Finally we will use the postselected state $|\chi_{x_f}\rangle$ employed above, defined by Eq. (27), that is a superposition of 2 narrow Gaussians centered on x_f and with the momentum collimated along the directions joining $\mathbf{r}_f$ to the center of the slits.

In the weak coupling limit, each interaction (29) gives rise to the weak value

$$(k_a)^w(t_b) = \frac{\chi^*_{x_f}(x_a,t_b)(-i\hbar\partial_{x_a})\left(\psi^1_{p_i^1}(x_a,t_b) + \psi^2_{p_i^2}(x_a,t_b)\right)}{\int dx\,\chi^*_{x_f}(x,t_b)\left(\psi^1_{p_i^1}(x,t_b) + \psi^2_{p_i^2}(x,t_b)\right)}, \tag{30}$$

similarly to Eq. (26). As we remarked above, the numerator of this expression should more realistically be integrated over the width $\Gamma(x)$ of the crystal. The important point here is that the polarization is rotated as a result of this interaction. For instance the interaction of a crystal at $\mathbf{r}_a$ with the photon in state $|\psi(t)\rangle|\nearrow\rangle$ for $t < t_b$ results after postselection in changing the polarization to

$$|P\rangle = e^{-i\gamma_a(k_a)^w}|H\rangle + e^{i\gamma_a(k_a)^w}|V\rangle, \tag{31}$$

where $|P\rangle$ stands here for the polarization state and where $\gamma_a = \int dt\, g_a/\hbar$. At postselection, this polarization state is read out by projecting $|P\rangle$ in a chosen basis; here we will employ the diagonal basis $\{|\nearrow\rangle, |\swarrow\rangle\}$. The polarization state thus encodes, similarly to the weak probe shifts in the ideal cases mentioned earlier, the past interactions with specific crystals. However, the difference is that in the ideal case with independent weak probes disposed on a grid, one could in principle read the shift indicated by each weak probe. Here, the rotation due to the interaction with each crystal cannot be read out since there are several crystals, each inducing a different rotation. The protocol we now detail circumvents this problem by introducing several steps in order to extract the weak rotations from the observed polarization intensities.

C. Protocol

In order to extract the weak values from the polarization intensities detected at postselection, we will introduce our protocol based on the setup shown in Fig. 8 involving four birefringent crystals. For definiteness we assume the initial and postselected states to be given by Eqs. (28) and (27) respectively. The protocol is not unique and its main idea can easily be adapted to other configurations.

Each of the four crystals interacts with the photon through a Hamiltonian given by Eq. (29), that we will write with an obvious notation $\hat{H}_A, \hat{H}_B$, etc. A (resp. C) is disposed close enough to slit 1 (resp. slit 2) so that the wave coming from the other slit has negligible amplitude. B and C are reached by waves coming from both slits. The idea underlying the protocol is to infer the rotation due to the interaction with each optical element. To do so, in a first step we place the crystal A only, so that $\hat{H}_A$ only comes into play. In a second step, we also place the crystal C and the resulting interaction Hamiltonian is $\hat{H}_A + \hat{H}_C$. In a third step, we insert in addition the crystals B and D. Finally, in a fourth step we place a phase shifter on crystal B, in order to create a π shift.

Let us denote by $|P_n\rangle$ the final polarization state after the realization of the nth step. We have

$$|P_1\rangle = \zeta(e^{-i\gamma_A(k_A)^w}|H\rangle + e^{i\gamma_A(k_A)^w}|V\rangle), \tag{32}$$

$$|P_2\rangle = \zeta(e^{-i\gamma_A(k_A)^w - i\gamma_C(k_C)^w}|H\rangle + e^{i\gamma_A(k_A)^w + i\gamma_C(k_C)^w}|V\rangle), \tag{33}$$

$$|P_3\rangle = \zeta(e^{-i\gamma_A(k_A)^w - i\gamma_C(k_C)^w - i\gamma_B(k_B)^w - i\gamma_D(k_D)^w}|H\rangle + e^{i\gamma_A(k_A)^w + i\gamma_C(k_C)^w + i\gamma_B(k_B)^w + i\gamma_D(k_D)^w}|V\rangle), \tag{34}$$

$$|P_4\rangle = \zeta(e^{-i\gamma_A(k_A)^w - i\gamma_C(k_C)^w + i\gamma_B(k_B)^w - i\gamma_D(k_D)^w}|H\rangle + e^{i\gamma_A(k_A)^w + i\gamma_C(k_C)^w - i\gamma_B(k_B)^w + i\gamma_D(k_B)^w}|V\rangle), \tag{35}$$

where $\zeta = \langle\chi_{x_f}(t_f)|\psi(t_f)\rangle/\sqrt{2}$. For each step the intensities in the diagonal basis, $I_n^{\nearrow} = |\langle\nearrow|P_n\rangle|^2$ and $I_n^{\swarrow} = |\langle\swarrow|P_n\rangle|^2$ are measured. From these intensities we can recover the rotations (or the weak values if the effective couplings γ_a are known, e.g., from calibration). Indeed, introducing the contrast C_n as

$$C_n = \frac{I_n^{\nearrow} - I_n^{\swarrow}}{I_n^{\nearrow} + I_n^{\swarrow}}, \tag{36}$$

the weak values $(k_A)^w$ and $(k_C)^w$ can be inferred from

$$\gamma_A(k_A)^w = \tfrac{1}{2}\arccos(C_1), \tag{37}$$

$$\gamma_C(k_C)^w = \tfrac{1}{2}\arccos(C_2) - \gamma_A(k_A)^w, \tag{38}$$

whereas the weak values $(k_B)^w$ and $(k_D)^w$ are deduced from

$$\gamma_B(k_B)^w = \tfrac{1}{2}[\arccos(C_3) - \arccos(C_4)], \tag{39}$$

$$\gamma_D(k_D)^w = \tfrac{1}{2}[\arccos(C_3) + \arccos(C_4)] - 2\gamma_A(k_A)^w - 2\gamma_C(k_C)^w. \tag{40}$$

The knowledge of the weak values is not sufficient to identify the weak trajectories, because several trajectories (or families of trajectories) may contribute to a given weak value. In the present setup, the crystals A and C receive a wave from a single slit, essentially emanating from the center of slits 1 and 2 respectively. So observing nonvanishing weak values $(k_A)^w$ and $(k_C)^w$ is a signature of the paths linking each slit to $\mathbf{r}_f$ (see the purple paths in Fig. 8). For the crystals B and D, however, we are in the situation described in Sec. IV C: as pictured in Fig. 8, each of these crystals receives a wave from each slit, a wave carried by the path from the center of the slit to the crystal (the neighboring paths also contribute, but the path at the slit center has the highest amplitude). In order to parse the contribution coming from each slit, we write

$$(k_B)^w = \left(k_B^{11}\right)^w + \left(k_B^{12}\right)^w, \tag{41}$$

$$(k_D)_w = \left(k_D^{22}\right)^w + \left(k_D^{21}\right)^w, \tag{42}$$

where

$$\left(k_a^{jl}\right)^w = \frac{\Xi^*_{x_f,p_j}(x_a,t_b)(-i\hbar\partial_{x_a})\psi^l_{p_i^l}(x_a,t_b)}{\sqrt{2}\int dx\, \chi^*_{x_f}(x,t_b)\left(\psi^1_{p_i^1}(x,t_b) + \psi^2_{p_i^2}(x,t_b)\right)}. \tag{43}$$

We have assumed in writing Eqs. (41) and (42) that each Gaussian $\Xi_{x_f,p_j}(x_f,t_f)$ of the postselected state χ_{x_f} remains narrow so that Ξ_{x_f,p_1} only filters the waves coming from B and Ξ_{x_f,p_2} only filters the waves coming from D. Under these conditions, we see that the rotation induced by $(k_B^{11})^w$ is a signature of the "direct" path going from slit 1 to $\mathbf{r}_f$ (represented in purple in Fig. 8) whereas $(k_B^{12})^w$ is due to the path going from slit 2 to B and from B to $\mathbf{r}_f$ (shown in green in Fig. 8). Similarly $(k_D^{22})^w$ is a signature of the path linking slit 2 to $\mathbf{r}_f$ while $(k_D^{21})^w$ singles out the path slit $1 \to \mathrm{D} \to \mathbf{r}_f$.

In order to extract the quantities defined in Eqs. (41) and (42) from experimental observations, we need the intensities with one or the other slit closed. Doing so changes the preselected state to either $\psi^1_{p_i^1}(x, t=0)$ or $\psi^2_{p_i^2}(x, t=0)$. Assume

only slit $l = 1, 2$ is open. The weak values due to the weak couplings at B and D, denoted κ_B^l and κ_D^l are given by

$$\kappa_B^l = \frac{\Xi^*_{x_f,p_1}(x_B,t_B)(-i\hbar\partial_{x_B})\psi^l_{p_i^l}(x_B,t_B)}{\int dx\, \chi^*_{x_f}(x,t_B)\psi^l_{p_i^l}(x,t_B)}, \tag{44}$$

$$\kappa_D^l = \frac{\Xi^*_{x_f,p_2}(x_D,t_D)(-i\hbar\partial_{x_D})\psi^l_{p_i^l}(x_D,t_B)}{\int dx\, \chi^*_{x_f}(x,t_B)\psi^l_{p_i^l}(x,t_B)}. \tag{45}$$

These single-slit weak values κ_a^l are obtained from intensity measurements similarly to the method employed in order to observe the weak values $(k_a)^w$ (see details in the Appendix).

We now note that the weak values κ_a^l can be written in terms of the quantities defined in the right-hand side of Eqs. (41) and (42). For example

$$(k_B)^w = \kappa_B^1 \frac{\langle\chi(t_f)|\psi^1_{p_i^1}(t_f)\rangle}{\langle\chi(t_f)|\psi(t_f)\rangle} + \kappa_B^2 \frac{\langle\chi(t_f)|\psi^2_{p_i^2}(t_f)\rangle}{\langle\chi(t_f)|\psi(t_f)\rangle}; \tag{46}$$

the same expression holds for $(k_D)^w$, so that the amplitude ratios in Eq. (46) can be obtained from the independent measurements of $(k_B)^w$, $(k_D)^w$, κ_B^1, κ_B^2, κ_D^1, and κ_D^2. From there the terms in Eqs. (41) and (42) are recovered, e.g., $(k_B^{11})^w = \kappa_B^1[\langle\chi(t_f)|\psi^1_{p_i}(t_f)\rangle/\langle\chi(t_f)|\psi(t_f)\rangle]$.

D. Weak trajectories from the observed weak values

The protocol combines weak values extracted from different setups, aimed at compensating the fact that rather than dealing with an array of weakly coupled probes, a realistic photonic experiment would rely on coupling the transverse momentum of the photon to its polarization when the photon interacts with a birefringent crystal.

When only one slit is open, say slit 1, the classical path linking the slit to the detection point $\mathbf{r}_f$ goes though A and B. This is captured by the interaction of the photon with the crystals placed at A and B through the rotation of the photon polarization encapsulated in the weak values $(k_A)^w$ and κ_B^1. When slit 2 is open, $(k_A)^w$ does not change, but κ_B^1 is modified to $(k_B)^w$: there is indeed an additional path taken by the photon reaching B from the source through slit 2. This "sum over paths" appears here by parsing $(k_B)^w$ as the coherent superposition given by Eq. (41). And of course there is also an additional path reaching the screen at $\mathbf{r}_f$ through slit 2, points C and D. This weak trajectory is evidenced by $(k_C)^w$ (that becomes nonzero as slit 2 is opened) and by the change of the polarization due to the interaction of the photon with the crystal placed at D [as a result the weak value changes from κ_D^1 to $(k_D)^w$]. Finally, if we close slit 1, the corresponding weak trajectories disappear, and this is evidenced by the the change in the polarization detected at postselection [$(k_A)^w$ becomes 0, $(k_B)^w$ and $(k_D)^w$ become κ_B^2 and κ_D^2, while $(k_C)^w$ remains the same].

VI. DISCUSSION AND CONCLUSION

The quantum formalism explains interferences in Young's double-slit setup by asserting the particle's wave function goes through both slits. In Feynman's path integral formulation, the waves that interfere are "carried" by classical trajectories, so that the interference figure is seen as due to a sum over paths. We have discussed how this path superposition could in principle be observed by implementing weak measurements between the particle and an array of weakly coupled probes, provided the particle can be appropriately postselected. The shifted probes reveal a coarse-grained form of the sum over paths in terms of "weak trajectories." We further proposed a concrete protocol in order to observe weak trajectories in a simple photonic double-slit setup containing a small number of crystals placed between the slits and the detector plane.

It should be emphasized that the specific form chosen for the weak measurement process is instrumental in sampling different aspects of the dynamics. A weak measurement of the momentum followed immediately by a projective position measurement leads to the velocity field associated with the Schrödinger current density. From there it is possible to reconstruct Bohmian trajectories [26], though as discussed elsewhere [11,27] Bohmian trajectories are not the observed quantities, contrary to the paths measured in this work that can be measured by following the wave function in space (through the position $\mathbf{r}_a$ of the probes) and time (by turning on and off the interaction at the desired time t_b). Indeed, in the case examined here, a weak interaction is not followed immediately by postselection (that would terminate the system's evolution), but it is followed by successive weak interactions, in order to sample the intermediate dynamics before detecting the particle on the screen. Note that strictly speaking photons do not admit Bohmian trajectories, so that single-photon trajectories reconstructed from experimentally obtained [15] weak values should be more appropriately related to the Poynting energy flow [28].

Another crucial aspect is the choice of postselection: the postselected wave function filters the dynamical aspects that can be accessed at an intermediate time. This aspect appeared in our scheme through collimation along one or two directions upon postselection (in order to filter the waves coming from a specific direction). It is also possible to consider postselecting coherently and simultaneously in distinct locations [10,29], rather than along distinct average momenta.

An interesting aspect that could be examined is the interplay between which-path information and the sum over paths. While the probe shifts due to the weak interactions can be understood as evidence that the quantum particle went through both slits [30], it is also possible to obtain which-slit information by tagging into orthogonal polarization states the paths that came from distinct slits. Moreover, it should be possible to implement a weak-value-based partial quantum erasure procedure [9,31] to recover a partial interference.

To sum up, we have proposed a method based on minimally perturbing weak interactions in order to observe the paths superposition in a double-slit interferometer. We have discussed an ideal scheme, based on inserting an array of probes between the slits and the detection plane, as well as a simplified protocol in view of an implementation of the method with single photons.

APPENDIX: MEASURING THE SINGLE-SLIT WEAK VALUES IN THE PHOTONIC PROTOCOL

We consider four distinct experimental schemes in order to measure the weak values κ_B^l and κ_D^l where $l = 1, 2$ designates

the open slit. As in the two-slit setups, the initial polarization is taken to be $|\nearrow\rangle$, the interaction Hamiltonians between the photon and the crystals are $\hat{H}_B$ and $\hat{H}_D$ [see Eqs. (28) and (29)], and the postselected also remains the same [Eq. (27)]. Only the preselected state is of course different, given by either $\psi^1_{p_i^1}(x, t = 0)$ or $\psi^2_{p_i^2}(x, t = 0)$.

With slit 1 open and crystals B and D in place, in a first setup the interaction seen by a photon is $\hat{H}_B + \hat{H}_D$; the resulting polarization state after postselection is

$$|P_1'\rangle = \langle \chi_{x_f}(t_f)\big|\psi^1_{p_i^1}\big\rangle (e^{-i\gamma_B\kappa_B^1 - i\gamma_D\kappa_D^1}|H\rangle + e^{i\gamma_B\kappa_B^1 + i\gamma_D\kappa_D^1}|V\rangle). \tag{A1}$$

Then we change the setup by adding a phase shifter to the D crystal and the final polarization state is

$$|P_2'\rangle = \langle \chi_{x_f}(t_f)\big|\psi^1_{p_i^1}\big\rangle (e^{-i\gamma_B\kappa_B^1 + i\gamma_D\kappa_D^1}|H\rangle + e^{i\gamma_B\kappa_B^1 - i\gamma_D\kappa_D^1}|V\rangle). \tag{A2}$$

We repeat the same steps but with slit 2 open instead. The polarization states are given by

$$|P_3'\rangle = \langle \chi_{x_f}(t_f)\big|\psi^2_{p_i^2}\big\rangle (e^{-i\gamma_B\kappa_B^2 - i\gamma_D\kappa_D^2}|H\rangle + e^{i\gamma_B\kappa_B^2 + i\gamma_D\kappa_D^2}|V\rangle), \tag{A3}$$

$$|P_4'\rangle = \langle \chi_{x_f}(t_f)\big|\psi^2_{p_i^2}\big\rangle (e^{-i\gamma_B\kappa_B^2 + i\gamma_D\kappa_D^2}|H\rangle + e^{i\gamma_B\kappa_B^2 - i\gamma_D\kappa_D^2}|V\rangle). \tag{A4}$$

As in Sec. V C, the polarization states are measured in the diagonal basis. Defining the contrast C_i' similarly to C_i in Eq. (36), we find the polarization rotations are given by

$$\gamma_B\kappa_1^B = \tfrac{1}{2}\arccos(C_1') + \tfrac{1}{2}\arccos(C_2'), \tag{A5}$$

$$\gamma_D\kappa_1^D = \tfrac{1}{2}\arccos(C_1') - \tfrac{1}{2}\arccos(C_2'), \tag{A6}$$

$$\gamma_B\kappa_2^B = \tfrac{1}{2}\arccos(C_3') + \tfrac{1}{2}\arccos(C_4'), \tag{A7}$$

$$\gamma_D\kappa_2^D = \tfrac{1}{2}\arccos(C_3') - \tfrac{1}{2}\arccos(C_4'). \tag{A8}$$

[1] Y. Aharonov, D. Z. Albert, and L. Vaidman, Phys. Rev. Lett. **60**, 1351 (1988).
[2] I. M. Duck, P. M. Stevenson, and E. C. G. Sudarshan, Phys. Rev. D **40**, 2112 (1989).
[3] A. Matzkin, Phys. Rev. Lett. **109**, 150407 (2012).
[4] A. Tanaka, Phys. Lett. A **297**, 307 (2002).
[5] T. Mori and I. Tsutsui, Prog. Theor. Exp. Phys. **2015**, 043A01 (2015).
[6] R. P. Feynman and A. R. Hibbs, *Quantum Mechanics and Path Integrals* (Dover, New York, 2010).
[7] L. S. Schulman, *Techniques and Applications of Path Integration* (Dover, New York, 2005).
[8] A. Matzkin, Phys. Rev. Research **2**, 032048(R) (2020).
[9] T. Mori and I. Tsutsui, Quantum Stud.: Math. Found. **2**, 371 (2015).
[10] L. P. Withers, Jr. and F. A. Narducci, J. Math. Phys. **56**, 062106 (2015).
[11] R. Flack and B. J. Hiley, Entropy **20**, 367 (2018).
[12] D. Georgiev and E. Cohen, Phys. Rev. A **97**, 052102 (2018).
[13] D. Katz, Int. J. Mod. Phys. A **34**, 1950033 (2019).
[14] Q. Duprey and A. Matzkin, Phys. Rev. A **95**, 032110 (2017).
[15] S. Kocsis *et al.*, Science **332**, 1170 (2011).
[16] D. H. Kobe, Ann. Phys. **123**, 381 (1979).
[17] M. Beau, Eur. J. Phys. **33**, 1023 (2012).
[18] M. Beau and T. C. Dorlas, Int. J. Theor. Phys. **54**, 1882 (2015).
[19] A. Zecca, Int. J. Theor. Phys. **38**, 911 (1999).
[20] H. Yabuki, Int. J. Theor. Phys. **25**, 159 (1986).
[21] A. Sinha, A. H. Vijay, and U. Sinha, Sci. Rep. **5**, 10304 (2015).
[22] A. Matzkin, Found. Phys. **49**, 298 (2019).
[23] In this case, the numerator in Eq. (25) should be replaced by $\int \chi^*_{x_f}(x', t_b)\psi^2_{p_i}(x', t_b)\Gamma_a(x')dx'$ where $\Gamma_a(\mathbf{r})$ gives the spatial profile of the interaction. For simplicity we have taken $\Gamma_a(\mathbf{r}) = \delta(\mathbf{r} - \mathbf{r}_a)$ throughout the paper.
[24] R. Bach, D. Pope, S.-H. Liou, and H. Batelaan, New J. Phys. **15**, 033018 (2013).
[25] U. Sinha, C. Couteau, T. Jennewein, R. Laflamme, and G. Weihs, Science **329**, 418 (2010).
[26] C. R. Leavens, Found. Phys. **35**, 469 (2005).
[27] A. Matzkin, J. Phys. A: Math. Theor. **48**, 305301 (2015).
[28] A. S. Sanz, M. Davidovic, M. Bozic, and S. Miret-Artes, Ann. Phys. **325**, 763 (2010).
[29] L. P. Withers Jr and F. A. Narducci, J. Phys. A: Math. Theor. **48**, 155304 (2015).
[30] H. F. Hofmann, T. Matsushita, S. Kuroki, and M. Iinuma, arXiv:2111.03203.
[31] M. Cormann, M. Remy, B. Kolaric, and Y. Caudano, Phys. Rev. A **93**, 042124 (2016).